Combining Multiplexed CRISPR/Cas9-Nickase and PARP Inhibitors Efficiently and Precisely Targets Cancer Cells



Soyoung Lee^{1,2}, Kyunghwan Kim^{1,3}, Hye-Jin Jeong², Subin Choi², Himchan Cheng², Dayoung Kim², Soomin Heo^{1,2}, Jinhee Mun², Minjong Kim⁴, Eunjin Lee², Yoon Ji Choi⁵, Seon-gyeong Lee⁶, Eun A Lee¹, Yewon Jang¹, Kayeong Lim⁷, Heon Seok Kim⁸, Euihwan Jeong^{6,9}, Seung-Jae Myung^{10,11,12}, Deok-Beom Jung¹¹, Chang Sik Yu¹³, In Ho Song¹³, M. Ryan Corces^{14,15,16}, Joo H. Kang², Kyungjae Myung^{1,2}, Taejoon Kwon^{1,2,6,9,17}, Tae-Eun Park², Jinmyoung Joo^{1,2,17}, and Seung Woo Cho^{1,2,17}

ABSTRACT

Triggering cancer cell death by inducing DNA damage is the primary aim of radiotherapy; however, normal cells are also damaged. In this study, we showed that delivery of only four synthetic guide RNAs with Cas9 endonuclease efficiently induced simultaneous DNA double-strand breaks, resulting in efficient cell death in a cell type–specific manner. Off-target effects of Cas9 endonuclease were prevented by using Cas9-nickase to induce DNA single-strand breaks and blocking their repair with PARP inhibitors (PARPi). When recombinant Cas9-nickase protein and multiple synthetic guide RNAs were delivered with PARPis into cultured cells, *in vivo* xenografts, and patient-derived

cancer organoids via lipid nanoparticles, cancer cells were unable to tolerate the induced DNA damage even in the presence of a functional *BRCA2* gene. This approach has the potential to expand the use of PARPis with verified safety and thus is a potentially powerful tool for personalized genome-based anticancer therapy.

Significance: Targeting cancer-specific variants with CRISPR/Cas9-nickase induces cancer-specific cell death in combination with DNA repair pathway inhibitors, demonstrating the potential of CRISPR cancer therapy for treating a broad range of cancers.

Introduction

Gene therapy is a promising therapeutic approach for diseases associated with heritable or somatic mutations for which current therapeutic approaches are intractable. By manipulating genomic DNA sequences or gene expression, gene therapy can alter the biological properties of live cells within patients for therapeutic purposes. The clustered regularly interspaced short palindromic repeat/ CRISPR-associated protein (CRISPR/Cas) system has benefits over more traditional gene-editing technologies and has become a powerful tool that enables specific and precise introduction of DNA modifications into living cells (1). It uses a synthetic guide RNA (sgRNA) oligonucleotide that directs Cas endonuclease to a specific target site in genomic DNA and then cleaves the targeted DNA region to trigger cell repair processes that introduce the desired genetic alteration (2–5). Whereas many CRISPR-based agents are

being developed for clinical use, most target specific variants of genes associated with diseases such as inherited monogenic disorders (6). However, the potential of CRISPR as a direct anticancer therapy remains largely unexplored.

Induction of excessive DNA damage that cancer cells cannot repair has been the main aim of anticancer treatment for more than a century (7). However, specific targeting of cancer cells to induce DNA damage is limited in the context of physical approaches such as radiotherapy, which frequently cause severe side effects due to undesired targeting of normal cells. To specifically target cancer cells, proteins such as BCR/ABL and HER2, which are specifically expressed in cancer cells, are targeted by anticancer therapy with imatinib (8) and trastuzumab (9), respectively. Additionally, the lack of biological pathways due to cancer-specific mutations enables the specific targeting of cancer cells. For example, the PARP inhibitor

¹Center for Genomic Integrity, Institute for Basic Science, Ulsan, Republic of Korea. ²Department of Biomedical Engineering, College of Information and Biotechnology, Ulsan National Institute of Science and Technology, Ulsan, Republic of Korea. ³Department of Chemistry, College of Natural Science, Ulsan National Institute of Science and Technology, Ulsan, Republic of Korea. ⁴Department of Biological Science, College of Information and Biotechnology, Ulsan National Institute of Science and Technology, Ulsan, Republic of Korea. 5 In Vivo Research Center, UNIST Central Research Facilities, Ulsan National Institute of Science and Technology, Ulsan, Republic of Korea. ⁶Division of Research and Development, CasCure Therapeutics, Seoul, Republic of Korea. ⁷Brain Science Institute, Korea Institute of Science and Technology, Seoul, Republic of Korea. ⁸Department of Life Science, College of Natural Science, Hanyang University, Seoul, Republic of Korea. ⁹CasCure Therapeutics, Ulsan, Republic of Korea. ¹⁰Department of Gastroenterology, Asan Medical Center, University of Ulsan College of Medicine, Seoul, Republic of Korea. 11 Digestive Diseases Research Center, University of Ulsan College of Medicine, Seoul, Republic of Korea, 12 EDIS Biotech, Seoul, Republic of Korea. ¹³Division of Colon and Rectal Surgery, Department of Surgery, Asan Medical Center, University of Ulsan College of Medicine,

Seoul, Republic of Korea. ¹⁴Gladstone Institute of Neurological Disease, San Francisco, California. ¹⁵Gladstone Institute of Data Science and Biotechnology, San Francisco, California. ¹⁶Department of Neurology, University of California San Francisco, San Francisco, California. ¹⁷Graduate School of Health Science and Technology, Ulsan National Institute of Science and Technology, Ulsan, Republic of Korea.

S. Lee, K. Kim, H.-J. Jeong contributed equally to this article.

Corresponding Authors: Seung Woo Cho, Ulsan National Institute of Science and Technology, 50 UNIST-gil, Ulju-gun, Ulsan 44919, Republic of Korea. E-mail: swcho@unist.ac.kr; Jinmyoung Joo, jjoo@unist.ac.kr; and Tae-Eun Park, tepark@unist.ac.kr

Cancer Res 2025;85:2890-904

doi: 10.1158/0008-5472.CAN-24-2938

This open access article is distributed under the Creative Commons Attribution-NonCommercial-NoDerivatives 4.0 International (CC BY-NC-ND 4.0) license.

©2025 The Authors; Published by the American Association for Cancer Research

(PARPi) olaparib is an effective anticancer drug for breast cancers with defective homologous recombination (HR) due to mutations in the *BRCA2* gene (10, 11). However, the use of targeted anticancer drugs is limited in cancer cells with mutations or altered expression levels of the targeted genes. Highly selective therapeutic approaches that directly target mutations of the cancer genome have not been developed.

When CRISPR induces double-strand breaks (DSB) specifically in the DNA of cancer cells and the corresponding DNA repair process is not performed appropriately, proliferation of cancer cells is inhibited, but normal cells lacking the target sequences are unaffected. A recent study found that although a single DNA DSB induced by CRISPR was cytotoxic, it did not kill cells (12). Several other studies reported that multiple DSBs induced by CRISPR efficiently kill mammalian (13–16) and plant (17) cells by increasing genomic instability. To achieve cancer cell–specific therapy, it is necessary to deliver as many as 10–30 cancer cell–specific sgRNAs, together with Cas9 endonuclease (Cas9^{WT}), to effectively kill cells. However, it is too challenging to select dozens of cancer-specific mutations and deliver all cancer cell–specific sgRNAs simultaneously to each cell for clinical applications.

Here, we demonstrate that intracellular delivery of multiplexed sgRNAs and Cas9WT in the form of ribonucleoprotein (RNP) efficiently induces cell death. We show that RNA-based delivery of CRISPR efficiently induces simultaneous DSBs; indeed, only four sgRNAs were required to efficiently kill cancer cells in vitro, as well as xenografted tumors in vivo and patient-derived organoids. Furthermore, to reduce unintended insertion/deletion (indel) mutations caused by multiplexed CRISPR in nontargeted cells lacking the target sequences, we induced multiple single-strand breaks (SSB) rather than DSBs by replacing Cas9WT with Cas9-nickase (nCas9^{D10A}; ref. 2). When repair of SSBs was inhibited by PARPis, cytotoxicity induced by multiplexed CRISPR/nCas9^{D10A} was retained, but indel frequencies were greatly reduced for each sgRNA. These results enable the development of precise anticancer therapies targeting cancer-specific variants and suggest that the applications of PARPis can be extended with CRISPR to the broad range of cancers lacking specific gene mutations.

Materials and Methods

Cell culture and transfection

HeLa (ATCC, CCL-2, RRID: CVCL_0030), HCT116 (ATCC, CCL-247, RRID: CVCL_0291), and MDA-MB-231 (ATCC, HTB-26, RRID: CVCL_0062) cells were cultured in DMEM (Gibco, #11965092). SW-480 cells (ATCC, CCL-228, RRID: CVCL_0546) were cultured in RPMI 1640 medium (Gibco, #11875093). All cell culture media were supplemented with 10% FBS (Gibco, #10082147) and 1% penicillin-streptomycin (Gibco, #15140122). Cells were cultured at 37°C in a humidified atmosphere containing 5% CO₂. Cell lines in this study, except the TP53 knockout (KO) HCT116 cell line, were obtained from and authenticated by the ATCC. The TP53 KO HCT116 cell line was provided by the Center for Genomic Integrity of Institute for Basic Science. All cell lines were maintained according to ATCC guidelines and regularly tested for Mycoplasma contamination using LookOut Mycoplasma PCR Detection Kit (Sigma-Aldrich, #MP0035). To deliver CRISPR RNPs or RNA, 0.5×10^4 cells were plated on a 24-well plate 1 day before transfection. For CRISPR RNP transfection, the following day, a Cas9WT RNP complex containing 665 ng of recombinant Cas9WT and 95 ng of sgRNAs was transfected into cells using Lipofectamine CRISPRMAX

Cas9 Transfection Reagent (Invitrogen, #CMAX00015). For CRISPR RNA (crRNA) transfection, 500 ng of Cas9^{WT} mRNA and 500 ng of sgRNAs were transfected into cells using Lipofectamine Messenger-MAX Transfection Reagent (Invitrogen, #LMRNA015). To ensure the best results, all cells were used within 20 passages.

Measurement of cell viability

Cell viability was measured using the CellTiter-Glo Luminescent Cell Viability Assay (Promega, #G7571). Transfected cells were incubated for 3 days and then detached using Trypsin-EDTA (0.25%; Gibco, #25200056). Cells were diluted with 400 μL of DMEM, and 100 μL of cells were aliquoted, mixed with 100 μL of CellTiter-Glo Reagent, and incubated for 10 minutes at room temperature. Luminescence signals were measured in white–opaque 96-well plates (Corning, #3917) using Infinite 200 (Tecan).

Colony formation assay

Cells were transfected with Cas9^{WT} or nCas9^{D10A} RNPs, incubated for 3 days, harvested using Trypsin-EDTA (0.25%), and plated on 6-well plates at the following densities: 100, 1,000, and 10,000 cells/well for HeLa cells and 30, 300, and 3,000 cells/well for HCT116 cells. The cell culture medium was changed every 5 days until 2 weeks after transfection. Then, cells were fixed with 4% paraformaldehyde for 20 minutes at room temperature, washed twice with PBS, stained with 0.005% crystal violet for 30 minutes, and washed with distilled water before scanning.

In vitro irradiation

Before 18 hours from transfection, 0.5×10^4 HeLa cells were seeded on a 24-well plate. CRISPR RNPs comprising 665 ng of recombinant Cas9^{WT} and 95 ng of sgRNAs were transfected into the cells using Lipofectamine CRISPRMAX Cas9 Transfection Reagent. Cells were irradiated at 0, 0.3, 1, 3, 10, or 30 Gy (Rad Source Technologies) 12 hours after transfection, and cell viability was measured 3 days after transfection.

In vitro transcription of gRNA and mRNA encoding SpCas9^{WT} or LbCas12a-ultra

In vitro-transcribed sgRNA for SpCas9WT and LbCas12a-ultra was synthesized from a DNA template containing a T7 promoter and sgRNA sequence using HiScribe T7 Quick High Yield RNA Synthesis Kit (NEB, #E2050S). A DNA template was produced by extension PCR using 100 µmol/L of each primer and NEBNext High-Fidelity 2X PCR Master Mix (NEB, #M0541L). With the DNA template, sgRNA was synthesized according to the manufacturer's standard RNA synthesis protocol. To synthesize Cas9 WT mRNA, a DNA template was generated by cutting p3s-Cas9HC (Addgene, #43945, RRID: Addgene_43945) with SpeI-HF (NEB, #R3133S) and XhoI (NEB, #R0146S) restriction enzymes. Then, mRNA was synthesized using NEB HiScribe T7 ARCA mRNA Kit with tailing (NEB, #E2060S). All in vitro-transcribed RNAs were purified using a Monarch RNA Cleanup Kit (NEB, #T2040L) and evaluated by visualization on denaturing agarose gels or PAGE gels. Cas9WT mRNA was verified using sgRNAs targeting a single

Purification of recombinant Cas9^{WT}, nCas9^{D10A}, and LbCas12a-ultra

The pET-LbCas12a-ultra vector was constructed using the DNA sequence encoding LbCas12a-ultra (18), which was cloned into the pET28a+ vector (Addgene, #69864-3). pET-Cas9-HN was derived

AACRJournals.orgCancer Res; 85(15) August 1, 2025 **2891**

from p3s-Cas9-HN (Addgene, #104171, RRID: Addgene_104171). These vectors were transformed into the C3013 strain (NEB, #C3013I), and recombinant Cas9WT or LbCas12a-ultra protein was expressed at 25°C for 4 hours by addition of 0.5 mmol/L IPTG, followed by purification using Ni-NTA agarose beads (Qiagen, #30210). Purified recombinant proteins were dialyzed in dialysis buffer (20 mmol/L HEPES, 150 mmol/L KCl, 1 mmol/L DTT, and 10% glycerol) and then concentrated using an Amicon Ultra-4 50K filter unit (Millipore, #UFC8050). Concentrated proteins were analyzed by visualization on SDS-PAGE gels and then quantified by comparing their band intensities with that of a BSA standard.

Isolation of cell lines stably expressing Cas9^{WT}

To generate cell lines stably expressing Cas9WT, a lentivirus was prepared using lenti-SpCas9-Blast (Addgene, #104997, RRID: Addgene_104997) and transduced into HCT116, HeLa, and MDA-MB-231 cells followed by selection using blasticidin S HCl (10 μ g/mL for HCT116 cells, 2 μ g/mL for HeLa cells, and 4 μ g/ mL for MDA-MB-231 cells; Gibco, #A1113903) for 7 days. Polyclonal cells were plated into 96-well plates (average of 0.3 cells/well) and then cultured for 2 weeks. Monoclonal cells were selected according to their morphology, growth rate, and gene-editing efficacy, as measured in a T7E1 assay using various sgRNAs targeting a single locus (e.g., VEGFA, HPRT1, CCR5, and EMX1).

Lentivirus preparation and infection

Each oligonucleotide was cloned into a lentiviral vector designed to express sgRNA or short-hairpin RNA (shRNA; Addgene, #60955, RRID: Addgene_60955; modified by replacing EF1a-puro-T2A-BFP with CMV-puro-T2A-mCherry) or coexpression of sgRNA and Cas9 (Addgene, #52961, RRID: Addgene_52961; Supplementary Table S1). For virus production, 7.0×10^6 HEK293T/17 cells (ATCC, CRL-11268, RRID: CVCL_1926) were seeded on a 10-cm dish. The following day, 6 µg of lentiviral vectors expressing sgRNA, 4.5 µg of psPAX2 (Addgene, #12260, RRID: Addgene_12260), and 1.5 μg of pMD2.G (Addgene, #12259, RRID: Addgene_12259) were cotransfected with Lipofectamine 3000 Transfection Reagent (Invitrogen, #L3000015). The supernatant containing viral particles was collected 48 hours after transfection and filtered. Lentiviruses encoding individual sgRNAs were concentrated using a Lenti-X concentrator (Clontech, #631232). The viral titer was measured using Lentivirus qPCR Quantification Kit (Abcam, #ab289841). For virus infection, virus and polybrene (final concentration 4 µg/mL; Sigma-Aldrich, #H9268) were added to cells at 25% confluency. Fresh medium was added 24 hours after infection.

Treatment with CRISPR/Cas RNPs and PARPis

In total, 0.5×10^4 cells were mixed with 1 μ mol/L olaparib (AZD2281; Selleckchem, #S1060), 1 µmol/L rucaparib (Selleckchem, #\$4948), 0.1 µmol/L niraparib (MK-4827; Selleckchem, #\$2741), 2 µmol/L veliparib (ABT-888; Selleckchem, #S1004), or 10 µmol/L iniparib (BSI-201; Selleckchem, #S1087) and then seeded in 24-well plates. Cells were transfected with nCas9^{D10A} RNPs, containing 665 ng of nCas9^{D10A} and 95 ng of sgRNAs, the following day and incubated for 3 days. At the applied concentrations, each PARPi exhibited no observable toxicity, as measured by the CellTiter-Glo assav.

Measurement of DNA cleavage frequencies and gene expression levels by RT-qPCR

To measure DNA cleavage frequencies, genomic DNA was extracted from cells transduced with CRISPR/Cas9WT using DNeasy Blood & Tissue Kit (Qiagen, #69506). qPCR was conducted using PowerUp SYBR Green Master Mix (Applied Biosystems, #A25742), 30 ng of genomic DNA, and 500 nmol/L of each primer. To quantify expression of the BRCA2 gene, total RNA was purified from cells treated with various amounts of shRNA (19) or siRNA targeting BRCA2 (Bioneer, #675-2) for 96 hours using RNeasy Plus Mini Kit (Qiagen, #74134). RT-qPCR was then performed using AccuPower GreenStar RT-qPCR Master Mix (Bioneer, #K-6403), 300 ng of total RNA, and 500 nmol/L of each BRCA2 primer. The expression levels of the GAPDH gene were used for normalization. Plates were placed in a RT-PCR instrument (CFX96 Touch Real-Time PCR Detection System, Bio-Rad), and the standard cycling mode was used.

Assay for transposase-accessible chromatin using sequencing

Generation of assay for transposase-accessible chromatin using sequencing (ATAC-seq) data involved performing ATAC-seq of cell lines according to the Omni-ATAC-seq protocol. Briefly, HCT116 cells grown in DMEM were harvested, and 50,000 cells were lysed in cold lysis buffer (10 mmol/L Tris-HCl, pH 7.4, 10 mmol/L NaCl, 3 mmol/L MgCl₂, 0.1% NP-40, 0.1% Tween-20, and 0.01% digitonin). Nuclei were isolated by centrifugation at 500 \times g for 10 minutes at 4°C, and the supernatant was removed. These nuclei then underwent a transposition reaction in transposase reaction mix (25 μL of 2× TD buffer, 2.5 μL of Tn5 transposase (in-house cloned, 100 nmol/L final concentration), 16.5 μL of PBS, 1% digitonin, 10% Tween-20, and 5 µL of nuclease-free water). Transposed DNA was cleaned-up using DNA Clean and Concentrator-5 Kit (Zymo, #D4014). After qPCR, up to six additional cycles of PCR were performed using NEBNext High-Fidelity 2X PCR Master Mix (NEB, #M0541L) and custom primers for NextEra indexing. Cleaned-up libraries were then pooled for sequencing with the Illumina Nova-Seq 6000 System, with 151 paired-end reads. The quality of the resulting reads was verified using FASTQC (v0.11.9, RRID: SCR_014583). For ATAC-seq data processing, an in-house pipeline and the hg38 reference genome were used. High-quality reads were mapped with bowtie2 (v2.4.4, RRID: SCR_016368), and unwanted reads (including chrM and blacklist regions) were discarded. Duplicate reads were marked with Picard (v1.79, RRID: SCR_006525), and peaks were called using MACS2 (v2.2.7.1, RRID: SCR_013291), with the specific parameters "-nomodel -call-summits -nolamda -keepdup all -shift -75 -extsize 150 -q 0.01." To plot the ATAC-seq signal tracks, depth-normalized bigWig files were generated using a bin size of 50 bp, which were then displayed by the UCSC genome browser.

Prediction of Cas9WT activity

Information about the target sequence of Cas9WT is given in the following format: "4 bp flanking sequence + 20 bp protospacer + 3 bp PAM + 3 bp flanking sequence." This was used as input for DeepSpCas9 to predict the efficiency of Cas9WT at the target site. In addition to DeepSpCas9, inDelphi was used to predict the pattern of mutations induced by Cas9WT at a given target site.

Targeted sequencing and analysis

To measure indel frequencies induced by CRISPR, cells were harvested 3 days after transfection, and genomic DNA was extracted using DNeasy Blood & Tissue Kit (Qiagen, #69506). A DNA library for targeted sequencing was prepared using primers (Supplementary Table S1) containing Illumina adapter sequences. Next, the library was quantified and loaded onto the Illumina NextSeq 500 or NovaSeq X System, with 150 paired-end reads. Mutation frequencies at target sites were analyzed using CRISPResso2 (v2.2.12, RRID: SCR_024503) or CRISPRpic, which revealed no significant differences. Mutation frequencies were calculated from the read counts, which included modified indel or unmodified sequences. Sequences corresponding to the heterozygous allele were categorized as unmodified sequences.

Prediction of putative off-targets

Off-target sites for each sgRNA were selected using the CRISPOR tool (RRID: SCR_015935) for predicting off-targets scores. After generating a list of candidate off-target sites with fewer than five mismatches, candidate sites with an uncut (%) score >0.05% were further filtered. The top five candidate sites, as determined by the cutting frequency determination score, were then analyzed by targeted sequencing.

Sequencing of TP53 variants

Total RNA was extracted from MDA-MB-231, SW-480, HCT116, HFE-145, and HeLa cells using AccuPrep Universal RNA Extraction Kit (Bioneer, #K-3140), followed by synthesis of cDNA using RevertAid First Strand cDNA Synthesis Kit (Thermo Fisher Scientific, #K1621). A primer specific for *TP53* was synthesized by Bioneer. Gene expression was determined using AccuPower GreenStar RT-qPCR Master Mix (Bioneer, #K-6403) and normalized against values for the housekeeping gene *GAPDH*. cDNA synthesized from each cell line was sequenced using the Illumina iSeq 100 system.

Alkaline comet assay

The alkaline comet assay was performed using CometSlide (R&D Systems, #4250-200-03) according to the manufacturer's instructions. Briefly, a cell suspension in cold PBS was mixed with low-melting point agarose and maintained at 37°C. The mixture was then spread evenly on a CometSlide. After solidification of the agarose, the slides were immersed in prechilled lysis solution (R&D Systems, #4250-050-01) and incubated overnight at 4°C. The slides were then immersed for 1 hour at 4°C in fresh alkaline unwinding solution, followed by electrophoresis at 21 V for 1 hour at 4°C in alkaline solution. DNA in the CometSlide was stained for 2 hours at room temperature with SYBR Gold Nucleic Acid Gel Stain (Invitrogen, #S11494) and then visualized under a fluorescence microscope (Olympus, BX53). The tail moment was quantified using Comet analysis software (Trevigen).

Immunoblot analysis

Whole-cell extracts were isolated, and immunoblot analysis performed as previously described (20). Briefly, cells were incubated on ice for 1 hour in RIPA buffer (50 mmol/L Tris-HCl, pH 8.0, 150 mmol/L NaCl, 2 mmol/L EDTA, 1% Triton X-100, 0.1% sodium dodecyl sulfate, and 1% sodium deoxycholate) supplemented with Halt Protease and Phosphatase Single-Use Inhibitor Cocktails (Thermo Fisher Scientific, #78442) and benzonase nuclease (Enzynomics, #M018S), followed by sonication and centrifugation. Prior to immunoblotting, proteins were separated by SDS-PAGE and transferred to a nitrocellulose membrane, which was then blocked for 20 minutes at room temperature in 5% skim milk dissolved in TBS containing 0.1% Tween 20 (TBST), followed by overnight incubation in TBST at 4°C with the following primary antibodies anti-PARP1 (Abcam, #ab227244, RRID: AB_227244), anti-GAPDH

(SantaCruz, #sc-32233, RRID: AB_627679), anti-p53 (GENETEX, #GTX128135, RRID: AB_2864277), anti-53BP1 (Abcam, #ab21083, RRID: AB_722496), and anti-phosphohistone H2AX (Ser139; Merck Millipore, #05-636, RRID: AB_309864). After washing, the membranes were incubated for 1 hour at room temperature with horseradish peroxidase (HRP)-conjugated secondary antibodies (Enzo Life Sciences, #ADI-SAB-300-J, RRID: AB_11179983) diluted at 1:5,000 in TBST. Protein signals were detected using enhanced chemiluminescence reagents (SuperSignal West Dura; Thermo Fisher Scientific, #37071) and visualized using an automated imaging system (ChemiDoc, Bio-Rad Laboratories).

Preparation and characterization of lipid nanoparticle formulations

For RNP delivery, lipid nanoparticles (LNP) were prepared using the ethanol dilution method modified from a literature record. All lipids (the molar ratio of LNPs was fixed with a C12-200/DOPE/ cholesterol/DMG-PEG/DOTAP ratio of 35/16/46.5/2.5/11.11) were dissolved in ethanol, and RNPs (with a molar ratio of sgRNA to Cas9 protein of 1:1) were dissolved in PBS (pH 7.4). These two solutions were rapidly pipetted and mixed at a PBS to ethanol ratio of 3:1 (v/v) and a total lipid to sgRNA ratio of 20:1 (w/w) and then incubated for 15 minutes at room temperature. For in vivo experiments, the RNP-loaded LNP formulations were purified using a dialysis kit (Pur-A-Lyzer Midi Dialysis Kit, MWCO 3.5 kDa) against PBS for 2 hours, concentrated with an Amicon Ultra-15 centrifugal filter (MWCO 50 kDa), and then intratumorally injected (50 µg of sgRNA-loaded LNPs per injection). To observe the morphologic structure of the lipid complex, RNP-loaded LNPs were dropped onto a carbon-coated grid for transmission electron microscopy analysis. After drying under ambient conditions, negative staining was performed using 2% uranyl acetate solution, followed by washing with distilled water. Transmission electron microscopy imaging was performed using a JEM-2100 instrument (accelerating voltage of 200 kV). The hydrodynamic size distribution was measured using Zetasizer Nano ZS (Malvern Instruments). C12-200 was purchased from Cayman Chemical. Olaparib was purchased from MedChemExpress. DOPE, DOTAP, and DMG-PEG (MW 2000) were purchased from Avanti Polar Lipids. Cholesterol, Pur-A-Lyzer Midi Dialysis Kit (MWCO, 3.5 kDa), and an Amicon Ultra-15 centrifugal filter (MWCO, 50 kDa) were purchased from Sigma-Aldrich. All chemicals were used without further purification.

In vivo sgRNA transfection into a Cas9-expressing HCT116 cell xenograft model

Invivofectamine 3.0 (Thermo Fisher Scientific) was used to deliver sgRNA according to the manufacturer's instructions with slight modifications. Although the product is intended for encapsulation and transfection of oligonucleotides such as siRNA or miRNA in vivo, sgRNA was also readily loaded due to its strong anionic characteristics. Equal volumes of sgRNA (12 mg/mL in nuclease-free water) and complexation buffer were mixed and then mixed with Invivofectamine 3.0 at a 1:1 (v/v) ratio. After gentle vortexing, the mixture was incubated at 50°C for 30 minutes for efficient encapsulation and then stored at 4°C until use.

Experimental animals and the tumor xenograft model

Female BALB/c nude mice (5 weeks old; RRID: MGI:2161072) were purchased from Orient Bio and used for all animal experiments. All animal experiments were approved by the Institutional Animal Care and Use Committee at the Ulsan National Institute of Science

AACRJournals.org Cancer Res; 85(15) August 1, 2025 **2893**

and Technology (UNISTIACUC-23-09). For the xenograft model, 5×10^6 HCT116 cells (unmodified) and HCT116 cells stably expressing Cas9^{WT} were suspended in 60 μL of PBS (pH 7.4), mixed with 60 µL of Matrigel (BD Biosciences), and subcutaneously injected into the right flank of mice for RNP delivery and sgRNA transfection, respectively. Tumor volume and body weight were measured every other day. Tumor volumes were calculated using the following formula:

$$V = \frac{a \times b^2}{2}$$

in which *V* is the volume, *a* is the length of the long axis, and *b* is the length of the short axis.

Once the tumor size reached approximately 80 mm³, the mice were randomly divided into four groups: (i) PBS, (ii) nontarget sgRNA/Cas9WT-loaded LNPs, (iii) Hmix-4/Cas9WT-loaded LNPs, and (iv) MT-50/Cas9WT-loaded LNPs. To evaluate antitumor efficacy, tumor-bearing mice were anesthetized with 1.5% isoflurane and intratumorally injected with PBS or LNPs every other day (50 μg of sgRNA-loaded LNPs per injection). Treatment was performed from days 0 to 14 (eight injections in total), and mice were sacrificed on day 25. The tumor growth inhibition rate (%) was calculated using the following formula:

$$= \left(1 - \frac{V_{Day\,0,\,treatment} - V_{Day\,24,\,treatment}}{V_{Day\,0,\,control} - V_{Day\,24,\,control}}\right) \times 100$$

in which V_{Day 0, treatment} and V_{Day 24, treatment} are the tumor volumes of the treatment groups at days 0 and 24 and VDay 0, control and V_{Day 24, control} are the tumor volumes of the PBS control group at days 0 and 24, respectively. Mice were sacrificed on day 25 for histologic analysis. To evaluate the efficacy of CRISPR/n $\overset{\checkmark}{C}$ as9 D10A with PARPis in vivo, Cas9WT was replaced with nCas9D10A without changing the LNP formulation. Before injection of RNP-loaded LNPs, olaparib (1.5 mg/kg; diluted in PBS) was injected intratumorally. To assess long-term therapeutic effects, six mice were prepared and subjected to a first round of treatment with Hmix-4/ Cas9WT-loaded LNPs from day 0 to day 14. The mice were then divided randomly into two groups: one group received an additional four injections of Hmix-4/Cas9 $^{\rm WT}$ -loaded LNPs, whereas the other group received four injections of PBS. The second round of treatment was performed from day 22 to day 28, with all injections administered every other day. The mice were sacrificed on day 33.

TUNEL assay

Whole-tumor tissues were fixed in 10% neutral-buffered formalin and then embedded in paraffin for sectioning at a thickness of 8 µm. Paraffin-embedded tumor sections were deparaffinized according to standard protocols. Heat-induced antigen retrieval was performed using a microwave with citrate buffer (pH 6.0, Sigma-Aldrich, #C9999-100ML), in a Coplin jar. Cellular apoptosis was analyzed using TUNEL Assay Kit-HRP-DAB (Abcam, following the manufacturer's instructions. Diaminobenzidine (DAB) solution detected the TdT labeling reaction in tumor tissue to identify DNA strand breaks generated during apoptosis. Hematoxylin counterstaining was performed to evaluate normal and apoptotic cells. To permanently preserve stained tissue, organic mounting buffer was used. Images were acquired using a virtual microscope (Olympus).

Ki-67 and caspase-3 IHC

Paraffin-embedded tumor sections (8 µm) were deparaffinized according to standard protocols. Heat-induced antigen retrieval was performed using a microwave with citrate buffer (pH 6.0, Sigma-Aldrich, #C9999-100ML), in a Coplin jar. Antigen-retrieved tissue sections were permeabilized with 0.4% Triton X-100. To evaluate proliferation, tissues were incubated overnight at 4°C with an anti-Ki-67 mAb (Santa Cruz, #sc-23900, RRID: AB_627859; diluted 1:200) followed by incubation for 2 hours at room temperature with an HRP-conjugated goat anti-mouse IgG (H+L) secondary antibody (Invitrogen, #31430, RRID: AB_228307; diluted 1:400). To evaluate apoptosis, tissues were incubated overnight at 4°C with an anti-caspase-3/p17/p19 mAb (Proteintech, #19677-1-AP, RRID: AB_10733244; diluted 1:100) followed by incubation for 2 hours at room temperature with an HRP-conjugated goat anti-mouse IgG (H+L) secondary antibody (Invitrogen, #31430; diluted 1:400). Signals were developed by application of DAB. Hematoxylin staining was performed to distinguish nuclear components. Stained tissues were preserved by addition of organic mounting buffer. Images were acquired using a BX51 optical microscope (Olympus). Quantification of IHC staining including TUNEL assay was performed using ImageJ software (NIH). The image analysis involved background subtraction, color deconvolution to isolate the DAB stain, appropriate thresholding, and measurement of positively stained areas. Quantitative results were presented as the percentage of positively stained areas relative to the total tissue area. Statistical comparisons between treatment groups were conducted using independent t tests. All IHC images and analyses were validated by a certified pathologist in blinded manner.

Delivery efficiency of the RNP complex

Tumor-bearing female BALB/c nude mice were prepared and divided into two groups. One group received a single intratumoral injection of nontarget sgRNA/Cas9WT-loaded LNPs, whereas the other received a single intratumoral injection of nontarget sgRNA/ Cas9WT-free RNP complexes. The mice were sacrificed at 3 hours after injection, and tumor tissues were collected. Each injection contained 50 µg of sgRNA and 250 µg of Cas9WT. To evaluate the efficiency of RNP delivery, paraffin-embedded tumor sections (8 µm) were deparaffinized following standard protocols, followed by heat-induced (microwave) antigen retrieval in citrate buffer (pH 6.0, Sigma-Aldrich, #C9999-100ML) in a Coplin jar. The antigen-retrieved tissue sections were permeabilized with 0.4% Triton X-100, incubated overnight at 4°C with an anti-CRISPR-Cas9 mAb (Abcam, #ab191468, RRID: AB_2692325), and then incubated for 2 hours at room temperature with an HRP-conjugated goat anti-mouse IgG (H+L) secondary antibody (Invitrogen, #31430; diluted 1:400). Signals were developed using DAB, and nuclear components were visualized by hematoxylin staining. The stained tissues were preserved with an organic mounting buffer, and images were captured using a BX51 optical microscope (Olympus).

Human cancer organoid culture

The colorectal cancer organoids used in this study were derived from tissues of patients diagnosed with colorectal cancer, which were obtained with approval from the Institutional Review Board of Asan Medical Center (Approval No. 2019-0340). The establishment of colorectal cancer organoids was also approved by the Institutional Review Board of Ulsan National Institute of Science and Technology (UNIST; approval no. UNISTIRB-18-49-A). All patients who underwent colorectal cancer resection surgery were fully informed

about the study and provided written informed consent prior to participation. As stated above, the study was approved by the institutional review boards of both institutions, UNIST and Asan Medical Center, and was conducted in accordance with the ethical guidelines outlined in the Declaration of Helsinki (World Medical Association). Resected colorectal cancer tissue segments larger than 1 cm³ were utilized to obtain suitable patient-derived cells for the generation of colorectal cancer organoids.

The colorectal cancer organoids were established following a published protocol (21) with slight modifications. The resected colorectal cancer segments, each measuring 1 cm³, were preserved in MACS Tissue Storage Solution (Miltenyi Biotec, #130-100-008) at 4°C and used within 8 hours of resection. The resected segments were first washed twice in Dulbecco's PBS (DPBS; Welgene, #LB001-02) without Ca²⁺/Mg²⁺ supplemented with 0.1 mg/mL Primocin (InvivoGen, #ant-pm-1) and 5 µg/mL Plasmocin (InvivoGen, #ant-mpp) to prevent contamination. Subsequently, the washed segments were fragmented into small pieces (2-5 mm²), vigorously washed in DPBS, and then incubated in a digestion buffer consisting of basal medium containing 1.5 mg/mL type II collagenase (Gibco, #17101015), 20 µg/mL hyaluronidase (Sigma-Aldrich, #H3506), and 10 μmol/L Y27632 (TOCRIS, #1254) at 37°C on a shaker for 1-3 hours. Following incubation, the isolated colorectal cancer cell clumps were transferred to fresh tubes at 1-hour intervals to maintain high cell viability, and 5% FBS was added to deactivate the enzymes. After centrifugation at 300 \times g for 5 minutes at 4°C, the cell clump pellet was resuspended in Matrigel (Corning, #354230) and seeded into nontreated 24-well cell culture plates (SPL, #32024; 50-µL droplet per well). Following solidification of Matrigel-containing colorectal cancer cells, which typically occurred approximately 20-30 minutes after seeding, colorectal cancer organoid culture complete medium (Supplementary Table S2) was applied to cover the Matrigel dome of colorectal cancer organoids. After 7 days of culture, the Matrigel dome containing embedded colorectal cancer organoids was harvested using DPBS and dissociated by treatment with TrypLE Express (Gibco, #12604021) for 5 minutes at 37°C. Following centrifugation at 250 \times g for 5 minutes at 4°C, the colorectal cancer cell pellet was obtained for transfection.

Delivery of CRISPR RNPs into cancer organoids

To deliver CRISPR RNPs, 0.8 × 10⁵ dissociated colorectal cancer organoid cells were suspended on an ultra-low attachment 24-well plate (Corning, #3473), and Cas9WT RNP complexes (containing 1.875 µg of recombinant Cas9WT and 0.27 µg of sgRNAs) or nCas9^{D10A} RNP complexes (containing 1.64 µg of $nCas9^{\rm D10A}$ and 0.23 μg of sgRNAs) were transfected into cells using CRISPRMAX (Invitrogen, #CMAX00008). Additionally, to observe the cytotoxicity of multiple DNA nicks induced by $nCas9^{\mathrm{D10A}}$ in the presence of PARP inhibition, dissociated colorectal cancer organoids were treated with 10 mmol/L olaparib (Selleckchem, #AZD2281) for 1 day before transfection. At 18 hours after transfection, cells were harvested in basal medium and centrifuged (250 \times g for 5 minutes at 4°C). The cell pellet was resuspended in 70 µL of Matrigel, and complete medium was added after solidification of Matrigel for 30 minutes. Transfected colorectal cancer organoids were cultured for 6 days and then detached using TrypLE Express, as described for the organoid dissociation process. Cell viability was measured using the CellTiter-Glo Luminescent Cell Viability Assay (Promega, #G7571). To measure cell viability in transfected colorectal cancer organoids, Matrigel-embedded colorectal cancer organoids were disrupted in 400 µL of DPBS by pipetting with a 200 μ L tip. Subsequently, 100 μ L of cells were aliquoted, mixed with 100 μ L of CellTiter-Glo Reagent, and incubated for 10 minutes at room temperature. Luminescence signals were measured in white–opaque 96-well plates (SPL, #30396) using a Synergy Neo2 multi-mode reader (BioTek).

Data availability

All raw sequencing data generated in the study are available via the Sequence Read Archive under accession number PRJNA1109424. All other raw data generated in this study are available upon request from the corresponding author.

Results

A limited number of multiplexed CRISPR/Cas efficiently kills cancer cells

To increase the utility of targeted cell death induced by CRISPR-based DNA damage, we aimed to reduce the number of sgRNAs required to be delivered into targeted cells. We hypothesized that simultaneous delivery of all desired sgRNAs to each cell is critical to trigger cell death induced by DNA DSBs (Fig. 1A). The timing of different DNA cleavages varies due to the multiple cellular processes required for sgRNA production, followed by formation of the Cas9^{WT}–sgRNA complex, which allows each DSB to be recognized and repaired individually. Lentiviral delivery of multiplexed sgRNA reduces the efficacy of the delivered sgRNAs (22), and the number of CRISPR-harboring viral particles that can be taken up by each cell is limited (23). Therefore, each sgRNA of the CRISPR system was intended to be pooled and delivered as RNA, which has higher transduction multiplicity than viral delivery.

To evaluate the efficacy of cell death after sgRNA transduction, we designed 18 sgRNAs (referred to as Hmix-18; Supplementary Table S3) that target indel mutations specific to the HCT116 colorectal cancer cell line and then prepared RNA by in vitro transcription (Supplementary Table S1) or a lentivirus encoding each sgRNA. Compared with a noncytotoxic sgRNA targeting the VEGFA locus, cell viability in response to a single sgRNA targeting 50 loci (referred to as MT-50) of the human genome decreased markedly after both RNA transfection and lentiviral infection. However, when the sgRNAs comprising Hmix-18 were pooled and delivered into the HCT116 cell line stably expressing SpCas9WT (Cas9WT derived from Streptococcus pyogenes), more rapid and marked cell death was induced when they were delivered by RNA transfection than when they were delivered by lentivirus infection (Supplementary Fig. S1A). When more than six sgRNAs were used, cell viability did not decline further. On day 9 after transfection, multiplexed CRISPR induced death in >90% of cells that underwent RNA transfection compared with 47% of cells that underwent lentivirus infection. We then examined the minimum number of sgRNAs required to trigger DSB-induced cell death. We found that when the sgRNA was highly active, only three sgRNAs were needed to induce marked cell death, whereas four sgRNAs (i.e., Hmix-4) were sufficient to induce efficient cell death specifically in the HCT116 cell line (Fig. 1B; Supplementary Table S3). Delivery of four sgRNAs targeting universal sequences within the human genome (Umix-4) was cytotoxic to multiple cell lines, including HeLa and MDA-MB-231 cells, although the potency of the cytotoxic effects varied between the cell lines (Supplementary Fig. S1B). In addition to delivering sgRNAs in the form of RNA, Cas9WT was also delivered as a recombinant protein or mRNA. Using this platform, we identified that CRISPR/Cas with Hmix-4 selectively decreased

AACRJournals.org Cancer Res; 85(15) August 1, 2025 **2895**

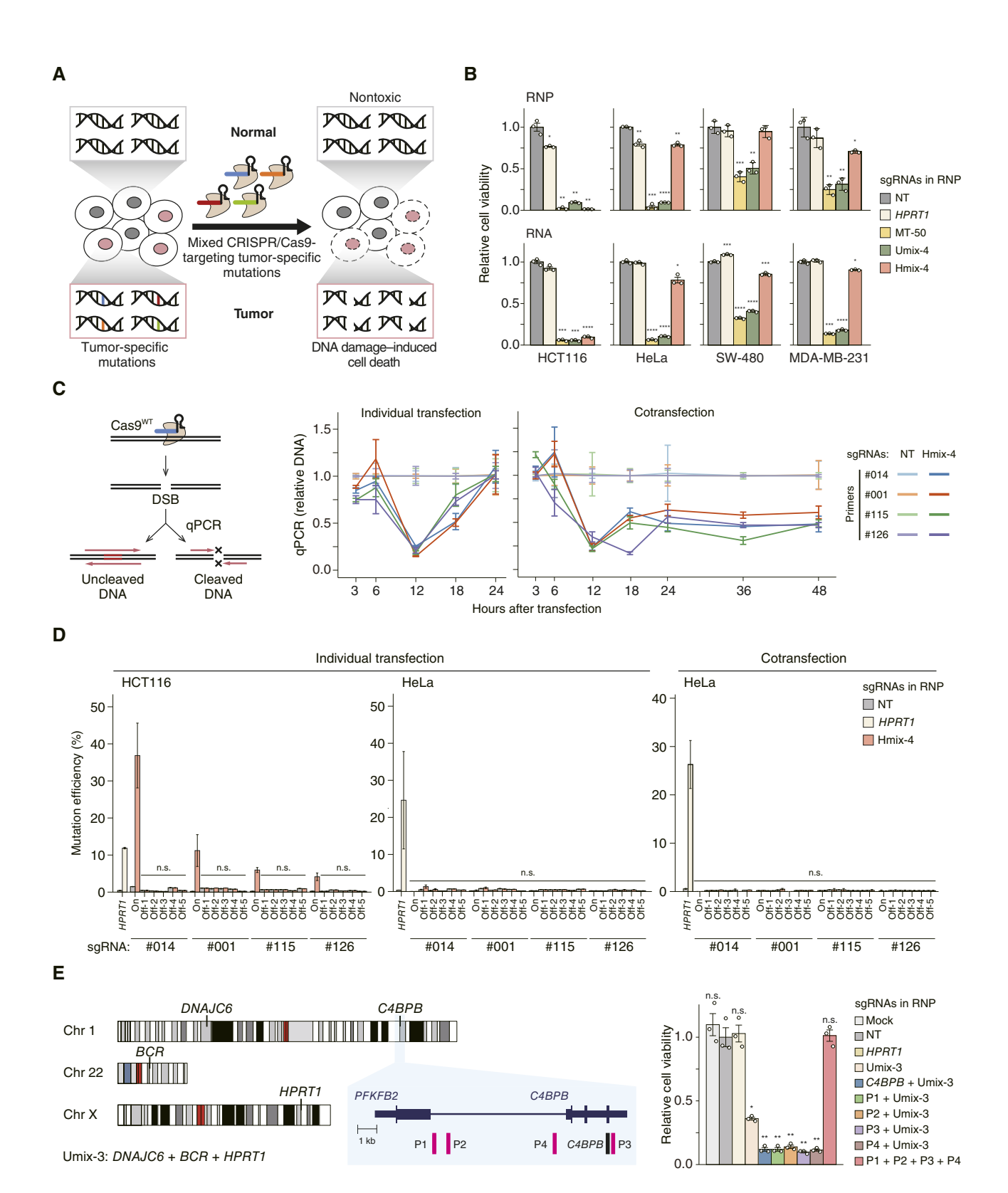


Figure 1. RNP-based delivery of multiplexed CRISPR/Cas induces cell death. A, Schematic of cancer-specific cell death induced by multiplexed CRISPR/Cas targeting cancer-specific indel mutations. B, Relative viability of HCT116, HeLa, SW-480, and MDA-MB-231 cells transfected with sgRNAs and Cas9WT protein (top) or mRNA (bottom). C, Left, schematic of qPCR to investigate relative cleavage of genomic DNA following (Continued on the following page.)

the viability of only HCT116 cells, whereas CRISPR/Cas with Umix-4 decreased the viability of all cell lines (Fig. 1B; Supplementary Fig. S2).

Simultaneous DSBs induced by multiplexed CRISPR/Cas are highly cytotoxic

To investigate differences between the delivery methods, we used two sgRNAs, placed 708 kb apart, which induce a large deletion in the human DMD gene for therapeutic purposes (24). When sgRNAs cleave two target sites, large deletions can be generated because the DNA ends are ligated; however, this is possible only when both targets are cleaved simultaneously. We performed qPCR of each target site, as well as the ligated junctions of large deletions, to measure DNA cleavage over time following sgRNA transduction. The efficiency of DNA cleavage at each target site was comparable using each sgRNA delivery platform (Supplementary Fig. S3; E44 and E56 primers). However, the large deletion was generated more rapidly and >2.4-fold more efficiently by RNP- or RNA-based delivery than by lentivirus-based delivery of CRISPR (Supplementary Fig. S3; DEL primer). Next, we analyzed simultaneous DSBs induced by Hmix-4 using qPCR. When each sgRNA in Hmix-4 was transfected separately, DSBs were generated 12 hours after RNP transfection and were completely repaired within 24 hours (Fig. 1C). However, when all four sgRNAs were delivered together, most DSBs remained unrepaired until 48 hours after transfection. These results suggest that RNP- or RNA-mediated delivery of CRISPR efficiently generates simultaneous DSBs, thereby reducing the number of sgRNAs required to inflict cytotoxic DNA damage.

To exclude the possibility of cell death due to unknown artificial effects, we first tested whether another CRISPR could kill cells as well as SpCas9WT. We used engineered Cas12a from Lachnospiraceae bacterium (LbCas12a-ultra) with its crRNA (18). When crRNAs were mixed and delivered as an RNP complex, LbCas12aultra induced cell death (Supplementary Fig. S4A). Importantly, $\mbox{SpCas9}^{\mbox{\scriptsize WT}}$ with the crRNA of LbCas12a-ultra was not cytotoxic. In addition, we noted that catalytically inactivated Cas9 (dCas9) did not induce cell death when used with Hmix-4 or Umix1-4 (Supplementary Fig. S4B). These findings suggest that CRISPR/Cas endonuclease-mediated DNA damage occurred at targeted loci to cause cytotoxicity and that cell death was not induced by the recombinant proteins or transcribed sgRNA itself. Next, we examined the possibility that a specific sgRNA among the multiplexed sgRNAs induced cell death by disrupting a gene essential for cell survival. To this end, we removed each sgRNA individually from the six sgRNAs (Hmix-6 and Umix-6) that effectively induced cell death and delivered the modified multiplexes individually into cancer cell lines (Supplementary Fig. S1). None of the six multiplexes, each

comprising five sgRNAs derived from Hmix-6 or Umix-6, restored cell viability (Supplementary Fig. S4C). Indeed, four sgRNAs targeting human reference sequences corresponding to Hmix-4 (Hmix-4R) were cytotoxic in HeLa, SW-480, and MDA-MB-231 cells, but not in HCT116 cells, supporting the notion that cytotoxicity is not dependent on the function of a specific mutation (Supplementary Fig. S4D). Multiplexed CRISPR induced cytotoxicity efficiently in noncancerous cell lines (Supplementary Fig. S4E), apoptosis-inhibitory p53-mutant cell lines, SW-480 and MDA-MB-231 cells (Supplementary Fig. S4F), and p53 KO HCT116 cells (Supplementary Fig. S4G). Although the sgRNAs comprising Umix-6 targeted human genes, none of these genes were essential for induction of cell death. Based on these results, we selected and transduced another multiplex comprising four sgRNAs (igHmix-4) from Hmix-18, which did not target genes or regulatory regions of the human genome (Supplementary Fig. S5A). This multiplex, which targets intergenic sequences, effectively induced death of HCT116 cells (Supplementary Fig. S5B and S5C). These findings suggest that multiplexed CRISPR-induced cell death is a general cellular response to DNA DSB damage, which is independent of the function of the target locus.

The endonuclease activity of Cas9^{WT} is crucial for CRISPR-induced cell death; therefore, we hypothesized that the DNA cleavage efficiency of Cas9^{WT} affects the overall efficacy of cell death. Accordingly, we designed 30 sgRNAs with various DeepSpCas9 scores, which predict the efficiency of CRISPR/Cas9^{WT} based on deep learning-based methods (25), and pooled groups of four sgRNAs in descending order of their DeepSpCas9 scores. Cell viability correlated strongly with the mean DeepSpCas9 score of the four sgRNAs transfected into HCT116 cells as RNPs (Supplementary Fig. S6A), rather than predicted mutation patterns (26) generated by CRISPR-induced DSB repair (Supplementary Fig. S6B). These data suggest that multiplexed CRISPR-induced cell death is caused by Cas9^{WT}-mediated DNA cleavage rather than by DNA mutations generated by cellular DNA repair.

Off-target effects are potentially a confounding factor, even if only a single sgRNA is delivered for CRISPR gene-editing (27, 28). Our approach involves delivery of multiple sgRNAs, and therefore the potential for off-target effects is compounded. To exclude this possibility, we conducted *in silico* analysis and selected five putative off-target sites predicted to be the most probable target of each sgRNA in Hmix-4 (29). We confirmed the induction of off-target mutations by targeted sequencing (Supplementary Table S4) upon both individual delivery of each sgRNA and simultaneous delivery. However, we did not detect any significant off-target mutations (Fig. 1D), potentially because mismatches were considered when designing these sgRNAs in addition to RNP-based delivery of

(Continued.) CRISPR/Cas9-mediated induction of DSBs. Relative cleavage of genomic DNA upon transfection of individual sgRNAs in Hmix-4 (middle) or cotransfection of four sgRNAs (right). The quantitative value was normalized to the nontarget locus corresponding to each target locus. **D,** Bar plots representing the mutation efficiency at on-target sites and five predicted candidate off-target sites for each sgRNA in Hmix-4. On-target sequences of Hmix-4 are not present in the genome of HeLa cells; therefore, 20-nt sequences adjacent to the PAM sequences according to the genomic coordinates were considered as on-target sequences and analyzed. Cas9^{WT} protein along with individual (left) or multiplexed (right) sgRNAs were transfected into HCTII6 or HeLa cells. The sgRNA targeting the *HPRTI* gene was used as a positive control for efficient RNP transfection. Mutation efficiencies were measured by targeted sequencing of each target site of Hmix-4. **E,** Chromosomal map of the four sgRNAs included in Umix-4. In the sky-blue box, the positions of the sgRNA targeting *C4BPB* and its neighboring sgRNAs are indicated (left). Relative viability of cells transfected with CRISPR/Cas9^{WT} targeting *C4BPB* and neighboring sgRNAs with Umix-3 (right). NT, nontarget control sgRNA. Umix, multiplexed sgRNAs targeting universally conserved human genome sequences. Hmix, multiplexed sgRNAs targeting HCTI16 cell–specific sequences. MT-50, a single sgRNA targeting 50 loci in the human genome. Cell viability was measured using the CellTiter-Glo assay at 72 hours after transfection and normalized to that observed following treatment with a nontarget sgRNA control. Error bars, the mean \pm SD of three independent biological replicates. In **B, D**, and **E**, statistical significance was calculated using an unpaired two-tailed Student t test: n.s., not significant (t), t0.00; t1, t2, t3, t3, t4, t5, t6, t7, t8, t8, t8, t9, t9,

AACRJournals.org Cancer Res; 85(15) August 1, 2025 **2897**

CRISPR (30). This is consistent with previous studies demonstrating that off-target mutations are highly dependent on target sequences and can be prevented by careful target site selection (31). This result indicates that the sgRNAs did not induce cell death via excessive offtarget activity.

Interestingly, delivery of multiplexed sgRNAs increases the genetargeting efficiency without causing significant cytotoxicity (32, 33). To further investigate this potential discrepancy, we designed four sgRNAs located close to the sgRNA targeting C4BPB, which markedly decreased cell viability in combination with Umix-3. We replaced the sgRNA targeting C4BPB with individual neighboring sgRNAs and found that each complex induced cell death with equivalent efficiency (Fig. 1E; Supplementary Fig. S7). However, delivery of neighboring sgRNAs together did not induce significant cell death. This suggests that the distribution of target loci, or their organization in the nucleus, is essential for DNA damage-induced cell death. Studying cellular responses based on three-dimensional distances within the genome is important to improve understanding of the effects of externally induced DNA damage. These results show that RNP-based delivery of multiplexed CRISPR/sgRNA mediates efficient and precise cell death through DNA damage in a targeted manner.

LNP-based CRISPR-RNP delivery induces targeted cell death

In addition to the potent cell death induced in vitro, we investigated whether multiplexed CRISPR/Cas9WT induces cancer cell death in vivo. To evaluate the in vivo efficacy of cell death induced by the four multiplexed sgRNAs, we used LNPs to deliver the CRISPR RNP complex (34) into tumor-bearing mice. HCT116 cells were subcutaneously injected into the right flank of nude mice and allowed to grow for 14 days until the tumors reached approximately 80 mm³. The CRISPR RNP complex composed of recombinant Cas9^{WT} protein and four sgRNAs (Hmix-4) was loaded securely into LNPs (Supplementary Fig. S8A), as verified by induction of HCT116 cell death and the DNA damage response in vitro (Supplementary Fig. S8B and S8C), and administered through intratumoral injections (Fig. 2A; Supplementary Fig. S8D). It should be also noted that significantly higher levels of Cas9 were found throughout the tumor tissues upon LNP-based intratumoral injection, whereas free RNP administration was retained hardly at all (Supplementary Fig. S8B). Tumor growth in mice treated with Hmix-4-containing RNPs was less than 33% of that in control mice (Fig. 2B). Tumor growth suppression reached up to 36% (Fig. 2C; Supplementary Fig. S8E) without prominent symptoms or safety concerns, and no notable changes in body weight during treatment were observed (Fig. 2D). To further investigate the effects of cell death on tumor tissues, we performed immunostaining for Ki-67 and caspase-3, as well as TUNEL histopathologic analysis of tumor sections after treatment. The levels of apoptotic cell death (caspase-3- and TUNEL-positive) and proliferating cells (Ki-67-positive) increased and decreased, respectively, in xenografts treated with CRISPR/Cas9WT (Supplementary Figs. S8F and S9). These results indicate that this treatment successfully induced DNA damage and subsequent apoptosis.

Additionally, we conducted targeted sequencing of each target site of Hmix-4 in the remaining HCT116 cell-derived xenografts at 25 days after injection. No mutations expected to be generated by CRISPR were detected (Fig. 2E), strongly suggesting that survival of residual cells was due to incomplete delivery of multiplexed CRISPR to all cancer cells comprising the tumor tissue rather than to

resistance. Additionally, we tested the in vivo efficacy of multiplexed CRISPR-induced cell death by delivering sgRNAs only using liposome nanoparticles, which have been verified for delivery of siRNA in vivo, to xenografts of HCT116 cells stably expressing SpCas9WT (Supplementary Fig. S10A). Overall observations were comparable with those made following LNP-mediated RNP delivery (Supplementary Fig. S10B-S10E), suggesting that tumor growth inhibition was not due to the delivery vehicle (i.e., LNPs). These results suggest that delivery of the multiplexed CRISPR RNP complex using LNPs efficiently induces targeted cell death in vivo.

Although intratumoral injection of the CRISPR RNP complex using LNPs was more efficient than injection of free RNPs, other challenges such as intracellular uptake and endosomal escape might be limiting factors, thereby preventing eradication of cancer cells and resulting in regrowth of tumor tissues over the long term (Fig. 2B). We verified that inefficient delivery of RNPs throughout the tumor lesion resulted in incomplete suppression of tumor growth. Additional experiments in which CRISPR RNP complexloaded LNPs were also administered via a second-round injection revealed that Hmix-4 CRISPR RNPs caused significant suppression of tumor growth in tumor-bearing mice (Supplementary Fig. S11A-S11D). In addition, the tumor suppression observed during the second round of RNP treatment emphasizes the feasibility of repeated administrations to target residual tumor cells. These data suggest that optimizing delivery vehicles to increase efficiency and retention at the tumor site could improve therapeutic outcomes significantly.

Multiplexed CRISPR/nCas9-nickase with PARPis is synthetic lethal to cancer cells

Induction of DSBs in the cell genome is a highly effective method. Although we did not detect any off-target mutations at putative offtarget sites, CRISPR can induce indel mutations or structural variations at unpredictable loci (35, 36). In human cells, DSBs are repaired mainly by error-prone nonhomologous end joining, leading to mutations (37). By contrast, SSBs are primarily repaired by PARP-mediated SSB repair, which is considered an error-free repair pathway (38). To investigate whether multiple induced SSBs are also lethal to cells, we replaced Cas9WT with nCas9D10A, which induces SSBs rather than DSBs.

Delivery of sgRNAs targeting four loci (Hmix-4 and Umix-4) with nCas9^{D10A} did not induce significant cytotoxicity (Fig. 3A), whereas less than 1% and 10% of HeLa and HCT116 cells, respectively, were viable with Cas9WT (Fig. 3B). PARP-mediated repair is suppressed by olaparib, a PARPi, and SSBs are repaired by HR (39). Blockade of both PARP-mediated repair and HR leads to cell death (10, 11). Thus, we hypothesized that PARPis would increase the cytotoxicity of multiple DNA nicks induced by nCas 9^{D10A} because a limited number of DSBs induced by Cas9WT efficiently kill cells proficient in the HR pathway. When multiplexed CRISPR/ nCas9^{D10A} complexes were delivered into cells with olaparib, Hmix-4 and Umix-4 were sufficient to induce cell death (Supplementary Fig. S12A and S12B), and this toxicity was not significantly different from that induced by CRISPR/Cas9WT (Fig. 3A and B). Treatment with a nontoxic dose of olaparib (1 µmol/L), which effectively inhibited PARylation (Supplementary Fig. S13A and S13B), showed greatly increased cytotoxicity when combined with multiplexed CRISPR/nCas9^{D10A} (Fig. 3C; Supplementary Fig. S12B). This lethality required both olaparib and the target sequences of CRISPR/ nCas9^{D10A}, meaning there were no effects with Hmix-4 in HeLa cells (Supplementary Fig. S13C). Indeed, treatment with nontoxic

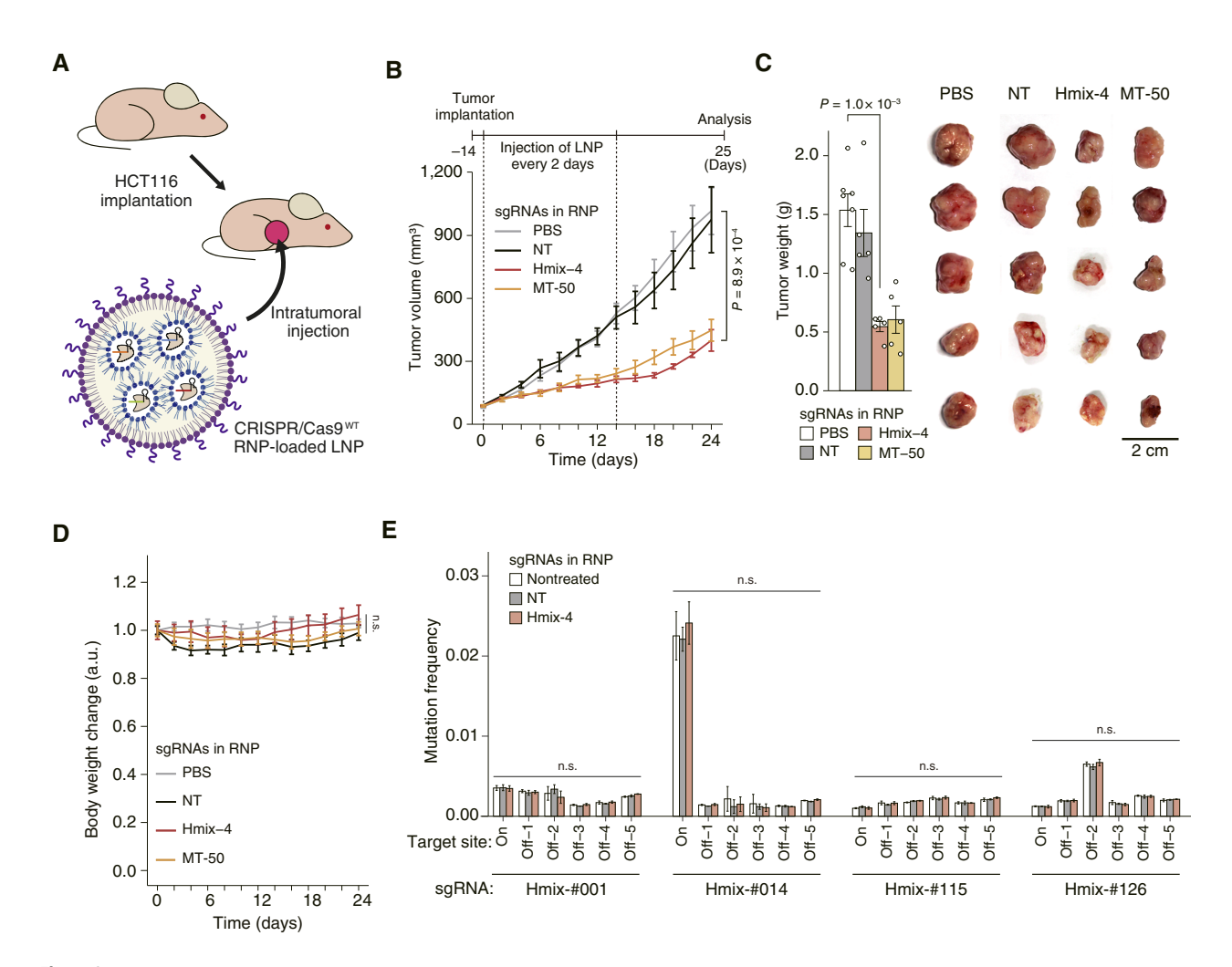


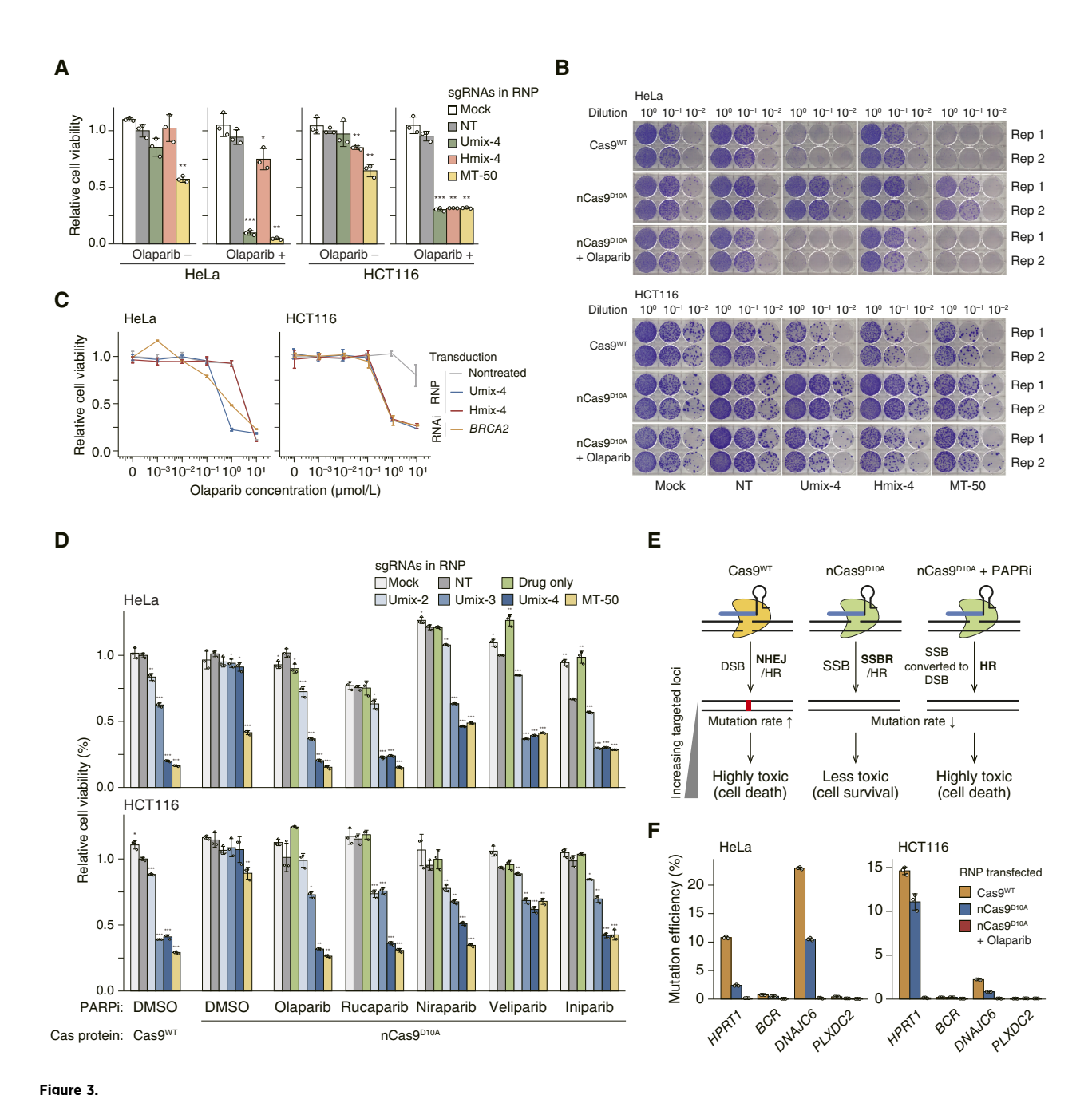
Figure 2. Assessment of *in vivo* antitumor effects in a mouse xenograft model after delivery of CRISPR-loaded LNPs. **A,** Schematic illustrating preparation of the mouse xenograft model for treatments and analyses. **B,** Timelines of treatments and tumor growth curve of HCT116 cell-derived xenografts in mice following administration of CRISPR/Cas9^{WT} RNP-loaded LNPs, which were delivered every 2 days (eight injections in total). Tumor volume was 80 mm³ at day 0. **C,** Weights and images of tumors obtained from mice at day 25 after the first injection. Scale bar, 20 mm. **D,** Body weight changes during the treatment period. In **B-D,** error bars indicate the mean \pm SE of independent biological replicates. Number of mice: n = 7 in the PBS group and n = 5 in the other groups. **E,** Mutation frequencies at on-target sites and five predicted candidate off-target sites for each sgRNA of Hmix-4 in remaining cancer cells in each mouse at 24 days after injection. Mutation frequencies were measured by targeted sequencing of each target site of Hmix-4. NT, nontarget control sgRNA. Error bars, mean \pm SD of three independent biological replicates. All statistical significance was calculated using an unpaired two-tailed Student t test; n.s., not significant ($P \ge 0.05$). **A,** Created in BioRender. Joo, J. (2025) https://BioRender.com/td206tx.

doses of other PARPis (40) also showed cytotoxicity with CRISPR/ nCas9^{D10A} (**Fig. 3D**). These results suggest that PARPis can be used with CRISPR/nCas9^{D10A} to induce death of cancer cells with any cancer-specific mutations, whereas the canonical synthetic lethality of olaparib depends on functional *BRCA2* expression (Supplementary Fig. S14A–S14C).

When delivering multiplexed CRISPR, it is possible that only some of them are delivered to cells or that cell death does not occur due to delivery of an insufficient amount of CRISPR. In such cases, it is expected that DNA lesions induced by nCas9^{D10A} are repaired through error-free DNA repair pathways, resulting in fewer indel mutations compared with Cas9^{WT} (41, 42). Indeed, in the presence of a PARPi, SSBs tend to be converted to DSBs during DNA replication and repaired by HR (10, 11, 43), which leads to a further decrease in indel mutations (**Fig. 3E**). As expected, indel frequencies

were lower upon treatment with nCas9^{D10A} and olaparib than upon treatment with nCas9^{D10A} alone (**Fig. 3F**). We reason that the multiple DSBs converted from SSBs are highly toxic to cells, as are DSBs directly induced by endonucleases. These results suggest that multiplexed CRISPR/nCas9^{D10A} with PARPis enables precise targeting of cancer cells with reduced off-target mutations.

To evaluate the efficacy of CRISPR/nCas9^{D10A} with PARPis for inducing cell death *in vivo*, we prepared LNPs containing CRISPR/nCas9^{D10A} and verified their potency with olaparib for inducing efficient cell death *in vitro* (Supplementary Fig. S15A). We then treated xenografts of HCT116 cells with LNPs and/or olaparib via intratumoral injection *in vivo*. CRISPR/nCas9^{D10A} with olaparib resulted in highly efficient tumor growth suppression (**Fig. 4A**; Supplementary Fig. S15B), even more than CRISPR/nCas9^{D10A} without olaparib. Importantly, tumor growth inhibition by CRISPR/nCas9^{D10A} with



Target-specific cell death induced by a combination of multiplexed CRISPR/nCas9D10A and PARPis. A, Relative viability of cells treated with multiplexed CRISPR/ nCas9^{DIOA} RNPs and 1 µmol/L olaparib. **B,** Colony formation assay using HeLa and HCTI16 cells transfected with multiplexed CRISPR/Cas9^{WT} or CRISPR/nCas9^{DIOA} RNPs, with or without 1 µmol/L olaparib. Cells were plated on 6-well plates at an initial density of 10,000 cells/well (HeLa cells) or 3,000 cells/per well (HCT116 cells), followed by serial dilution (10-fold). Each colony formation assay was performed in duplicate. The brightness of the images was adjusted for visibility. C, Relative cell viability in the presence of different concentrations of olaparib in combination with multiplexed CRISPR/nCas9DIOA RNPs. A siRNA or shRNA targeting the BRCA2 gene was used as a positive control for the synthetic lethality of olaparib. **D,** Cytotoxicity of PARPis combined with multiplexed CRISPR/nCas9^{DIOA} RNPs. NT, nontarget control sgRNA. **E,** A model for induction of cytotoxicity following CRISPR/Cas9^{WT} or CRISPR/nCas9^{DIOA} treatment. Bold text indicates the dominant repair pathways of each damage type. **F,** Mutation efficiency at each target sequence following transfection of RNPs containing each sgRNA and Cas9^{WT} or nCas9^{DIOA}, with or without olaparib treatment, into HeLa and HCT116 cells. Cell viability was measured in a CellTiter-Glo assay performed at 72 hours after transfection, and data were normalized to those observed following treatment with a nontarget sgRNA control. Error bars, mean ±SD of three independent biological replicates. All statistical significances were calculated using an unpaired two-tailed Student t test. *, P < 0.05; **, P < 0.01; ***, P < 0.001.

olaparib was comparable with that by CRISPR/Cas9WT (Fig. 4B; P = 0.731) without observable side effects or body weight loss (Supplementary Fig. S15C). Immunostaining for Ki-67 and caspase-3, as well as TUNEL histopathologic analysis of tumor sections after treatment, showed that the level of apoptotic cell death (caspase-3and TUNEL-positive) increased and the level of proliferating cells

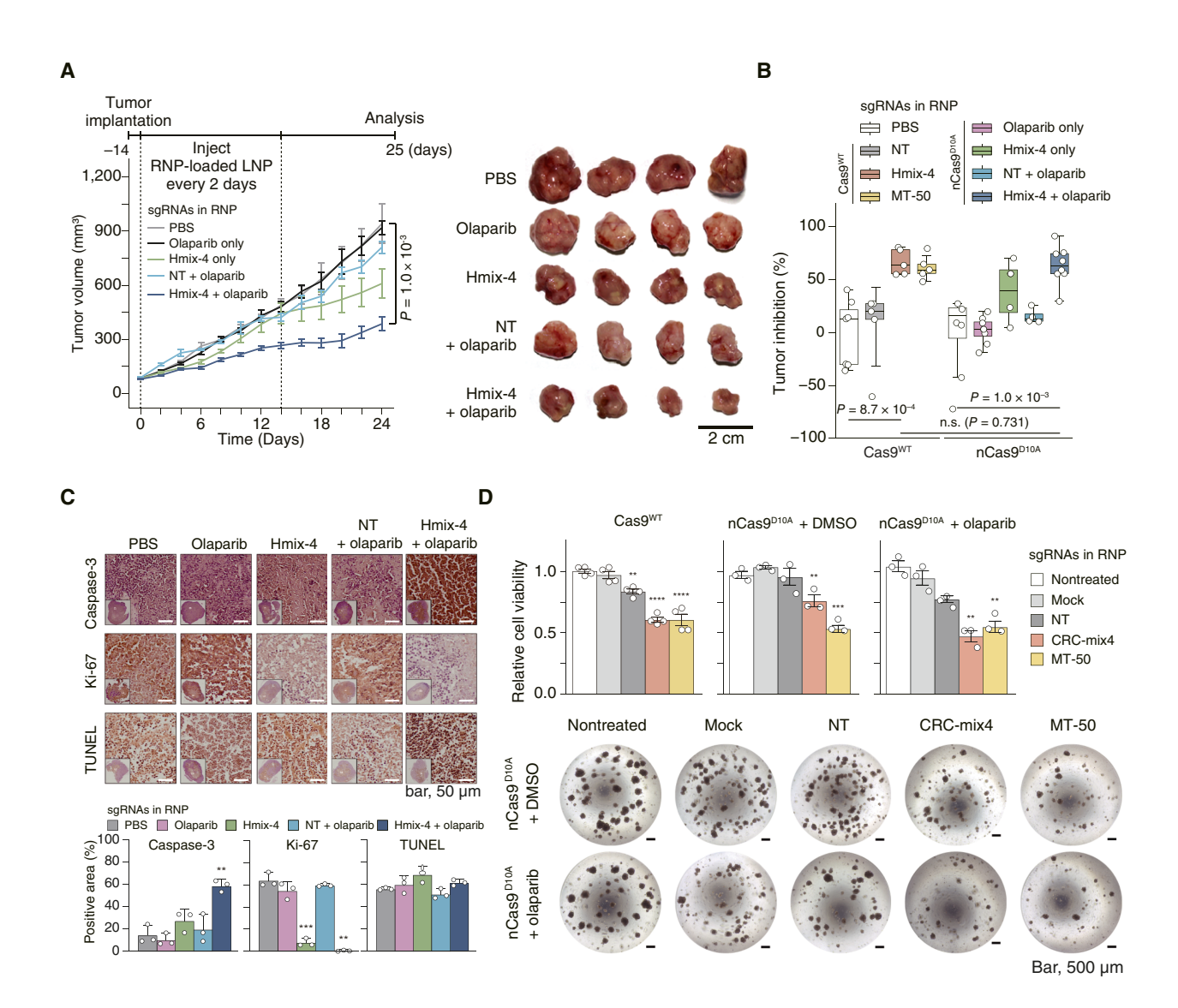
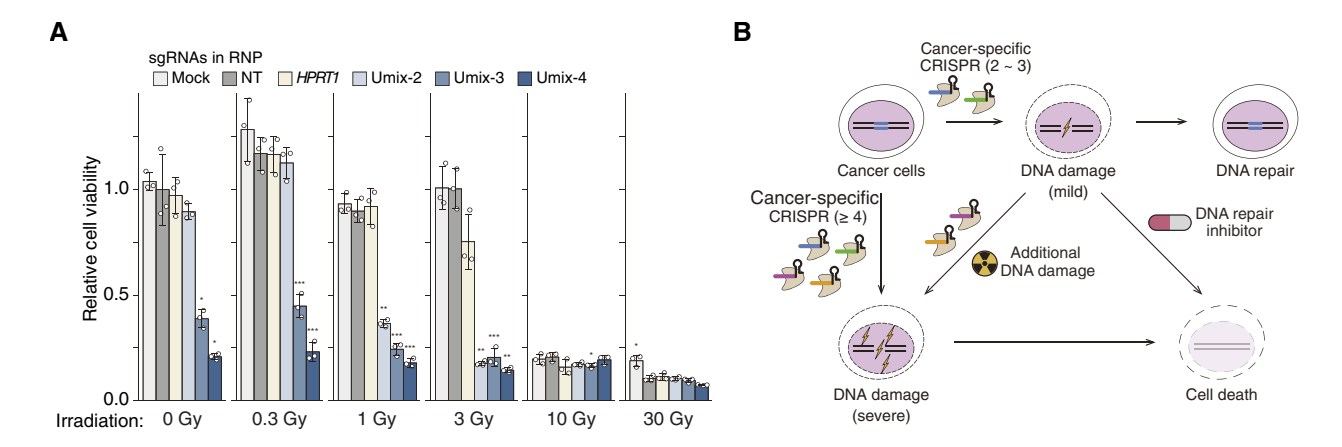


Figure 4. Evaluation of targeted cell death with multiplexed CRISPR/Cas9^{DIOA} and PARPis in a mouse xenograft model and human colorectal cancer organoids. **A,** Timeline of treatment and tumor growth curves for HCT116 cell-derived xenografts following administration of olaparib (1.5 mg/kg) and/or LNPs containing RNPs consisting of CRISPR/Cas9^{DIOA} and sgRNAs (delivered every 2 days; eight injections in total). Left, tumor volume was 80 mm³ at day 0. Right, images of tumors at day 25 after the first injection. Scale bar, 2 cm. B, Tumor growth inhibition following each treatment. C, IHC staining for caspase-3 and Ki-67 and a TUNEL assay in ex vivo tumor tissues. Bottom left, hematoxylin was used as a nuclear stain. The areas shown in the images are indicated by white boxes in the wholeslide images. Positive cells are stained brown. Scale bars, 50 µm. Quantitative analysis of the area positive for caspase-3, Ki-67, or TUNEL staining was performed using ImageJ software (bottom). Number of mice used for Cas9^{WT}: n = 7 in the PBS group and n = 5 in the other groups. Number of mice used for nCas9^{D10A}: n=6 in the PBS group, n=7 in the olaparib-only group, n=8 in the Hmix-4 with olaparib group, and n=4 in the other groups. **D,** Cell viability in human colorectal cancer organoids following transfection of multiplexed CRISPR RNPs along with Cas9 $^{\text{WT}}$ or nCas9 $^{\text{D10A}}$, with or without 1 μ mol/L olaparib. Scale bars, 500 μm. The CellTiter-Glo assay was performed at 6 days after transfection, and the results were normalized to a nontreatment control. Number of independent transfections: n = 4 for Cas9^{WT} and n = 3 for nCas9^{DIOA}. CRC-mix4, colorectal cancer-mix4; NT, nontarget control sgRNA. All statistical significances were calculated using an unpaired two-tailed Student t test. n.s., not significant; **, P < 0.01; ***, P < 0.001; ***, P < 0.0001. Error bars, mean \pm SE of biological replicates.

(Ki-67-positive) decreased in xenografts treated with CRISPR/ nCas9^{D10A} and olaparib, indicating that tumor growth was inhibited by induction of DNA damage and subsequent apoptosis (Fig. 4C; Supplementary Fig. S15D). When CRISPR/nCas9^{D10A} was introduced with olaparib into patient-derived colorectal cancer organoids, sgRNAs targeting cancer-specific mutations (colorectal cancer-mix4) in the patient's genome effectively inhibited organoid growth comparable with Cas9WT (Fig. 4D). These results suggest that cell death induced by targeted DNA damage using multiplexed CRISPR/ nCas9^{D10A} with a PARPi holds promise as a personalized therapeutic approach for patients with cancer.

In addition to the DNA repair inhibitors, we investigated whether the cytotoxic effect of multiplexed CRISPR could be enhanced by inducing additional DNA damage. At a radiation dose of 1 Gy,



Synthetic lethality of combined CRISPR/Cas9 and DNA damage-inducing treatments. A, Bar plots showing the viability of cells treated with multiplexed CRISPR/Cas9WT RNPs plus irradiation. Cell viability was measured using the CellTiter-Glo assay at 3 days after transfection, and data were normalized to those observed following treatment with a NT sgRNA control without irradiation. Cell viability was also measured at 72 hours after transfection, and data were normalized to those observed following treatment with a nontarget sgRNA control. Error bars, mean ± SD of three independent biological replicates. B, Schematic illustrating synthetic lethality of CRISPR/Cas9 targeting, followed by DNA damage-inducing treatment or DNA repair inhibitors such as additional CRISPR/Cas, irradiation, or a PARPi. NT, nontarget control sgRNA. Statistical significance was calculated using an unpaired two-tailed Student t test. *, P < 0.05; **, P < 0.01; ***, P < 0.001.

which does not cause cell toxicity alone, CRISPR-induced cytotoxicity was significantly enhanced (Fig. 5A). Notably, even with the use of only two sgRNAs, which alone do not reduce cell viability, cells could be effectively killed. These results suggest that a few of CRISPR targeting cancer-specific mutations can be effectively combined with existing DNA damage-based cancer therapies (Fig. 5B).

Discussion

The present study demonstrates that human cancer cells are sensitive to CRISPR-induced simultaneous DNA damage, which can induce cell death with only 3 to 4 sgRNAs targeting cell typespecific mutations. We further improved this method by replacing Cas9WT with nCas9D10A, which causes fewer unpredictable offtarget mutations. When SSB repair pathways are suppressed by PARPis, SSBs induced by multiplexed CRISPR/nCas9^{D10A} are not tolerated by human cells similar to induced DSBs. Importantly, the lethality of PARPis requires BRCA mutations to induce HR deficiency, and we showed that these mutations can be replaced by any mutations targetable with CRISPR/nCas9^{D10A}. This suggests that any emergent mutations are potential targets of this strategy, thereby providing additional treatment options even if cancer cells survive the initial treatment. Thus, PARPis can be applicable to a broad spectrum of patients with cancer. Furthermore, when delivered with CRISPR, PARPis or radiation showed toxicity at dose at which they did not show toxicity when used alone. Therefore, it may be possible to reduce the dosage of PARPis or radiation that show toxicity.

As a proof-of-principle, we delivered the CRISPR/Cas9 RNP complex via intratumoral injection, which facilitates robust evaluation of its potential to induce targeted DNA damage and cancer cell death and achieves high concentrations of the therapeutic agents directly at the tumor site while at the same time minimizing systemic toxicity. Although intratumoral injection has been utilized successfully in clinical trials for the delivery of oncolytic viruses, immune modulators, and gene-editing tools (42-44), developing advanced systemic delivery such as intravenous administration

using targeted LNPs (44) or virus-like particles (45-47) is critical for enhancing the translational potential of multiplexed CRISPR for cancer therapy due to its ability to reach both primary tumors and disseminated metastatic sites.

Taken together, these results suggest that combining multiplexed CRISPR with DNA repair inhibitors or DNA damaging reagents induces targeted synthetic lethality in cells with CRISPR target sequences, thereby increasing the feasibility of safe and precise anticancer therapy in a DNA-centric manner.

Authors' Disclosures

S. Lee reports a patent for PCT/KR2024/012084 pending. K. Myung reports a patent for PCT/KR2024/012084 pending and is a stockholder of CasCure Therapeutics, which licensed the original patent of CINDELA treatment for cancer, of which, he is an inventor. T. Kwon reports other support from CasCure Therapeutics outside the submitted work; in addition, T. Kwon has a patent for PCT/ KR2024/012084 pending. J. Joo reports nonfinancial support from CasCure Therapeutics during the conduct of the study. S.W. Cho reports grants from the South Korean government during the conduct of the study and other support from CasCure Therapeutics outside the submitted work; in addition, S.W. Cho has a patent for PCT/KR2024/012084 pending. No disclosures were reported by the other authors.

Authors' Contributions

S. Lee: Investigation, visualization. K. Kim: Investigation, visualization. H.-J. Jeong: Investigation, visualization. S. Choi: Investigation. H. Cheng: Investigation. D. Kim: Investigation, visualization. S. Heo: Investigation. J. Mun: Investigation. M. Kim: Investigation. E. Lee: Investigation. Y.J. Choi: Investigation. S.-g. Lee: Investigation. E.A. Lee: Investigation. Y. Jang: Investigation. K. Lim: Methodology. H.S. Kim: Methodology. E. Jeong: Investigation. S.-J. Myung: Methodology. D.-B. Jung: Methodology. C.S. Yu: Methodology. I.H. Song: Methodology. M.R. Corces: Methodology, writing-review and editing. J.H. Kang: Methodology, writing-review and editing. K. Myung: Conceptualization, supervision, writing-review and editing. T. Kwon: Conceptualization, supervision, writingreview and editing. T.-E. Park: Supervision, writing-review and editing. J. Joo: Conceptualization, supervision, visualization, writing-original draft, writing-review and editing. S.W. Cho: Conceptualization, supervision, visualization, writing-original draft, writing-review and editing

Acknowledgments

We thank members of the Genome Engineering Laboratory and Center for Genome Integrity of the Institute for Basic Science at UNIST for helpful discussions and assistance. We also thank Seokjoong Kim for helpful discussions and advice. We also acknowledge the UNIST Central Research Facility, especially the In Vivo Research Center for supporting the use of the equipment. We appreciate Song-Yi Choi, an expert pathologist in the Department of Pathology at Chungnam National University College of Medicine, for independently evaluating the data from IHC experiments. This work was supported by Institute for Basic Science grant IBS-R022-D1 (K. Myung); National Research Foundation of Korea Grant funded by the Ministry of Science and ICT of Korea RS-2024-00399800 (J.H. Kang, T.-E. Park, and S.W. Cho); National Research Foundation of Korea Grant funded by the Ministry of Science and ICT of Korea RS-2023-00213043 and RS-2024-00509412 (S.W. Cho); National Research Foundation of Korea Grant funded by the Ministry of Science and ICT of Korea RS-2023-00209822 (J. Joo); Basic Science Research Program through the National Research Foundation of Korea funded by

the Ministry of Education 2021R1A6A1A03040260 (S.-J. Myung); The Korea Health Technology R&D Project through the Korea Health Industry Development Institute and Korea Dementia Research Center, funded by the Ministry of Health & Welfare and Ministry of Science and ICT of Korea HU20C0094 (T.-E. Park and J. Joo); The Korea Health Technology R&D Project through the Korea Health Industry Development Institute, funded by the Ministry of Health & Welfare of Korea HI19C1095 (D. Kim); POSCO Science Fellowship of the POSCO TJ Park Foundation (J. Joo); and UNIST Research Fund 1.240016.01 (S.W. Cho).

Note

Supplementary data for this article are available at Cancer Research Online (http://cancerres.aacrjournals.org/).

Received August 15, 2024; revised January 16, 2025; accepted May 2, 2025; posted first May 6, 2025.

References

- Katti A, Diaz BJ, Caragine CM, Sanjana NE, Dow LE. CRISPR in cancer biology and therapy. Nat Rev Cancer 2022;22:259–79.
- Jinek M, Chylinski K, Fonfara I, Hauer M, Doudna JA, Charpentier E. A programmable dual-RNA-guided DNA endonuclease in adaptive bacterial immunity. Science 2012;337:816–21.
- Cho SW, Kim S, Kim JM, Kim JS. Targeted genome engineering in human cells with the Cas9 RNA-guided endonuclease. Nat Biotechnol 2013;31:230–2.
- Cong L, Ran FA, Cox D, Lin S, Barretto R, Habib N, et al. Multiplex genome engineering using CRISPR/Cas systems. Science 2013;339:819–23.
- Mali P, Yang L, Esvelt KM, Aach J, Guell M, DiCarlo JE, et al. RNA-guided human genome engineering via Cas9. Science 2013;339:823-6.
- 6. Mullard A. Gene-editing pipeline takes off. Nat Rev Drug Discov 2020;19:
- Connell PP, Hellman S. Advances in radiotherapy and implications for the next century: a historical perspective. Cancer Res 2009;69:383–92.
- Druker BJ, Talpaz M, Resta DJ, Peng B, Buchdunger E, Ford JM, et al. Efficacy and safety of a specific inhibitor of the BCR-ABL tyrosine kinase in chronic myeloid leukemia. N Engl J Med 2001;344:1031–7.
- Fendly BM, Winget M, Hudziak RM, Lipari MT, Napier MA, Ullrich A. Characterization of murine monoclonal antibodies reactive to either the human epidermal growth factor receptor or HER2/neu gene product. Cancer Res 1990;50:1550–8.
- Bryant HE, Schultz N, Thomas HD, Parker KM, Flower D, Lopez E, et al. Specific killing of BRCA2-deficient tumours with inhibitors of poly(ADP-ribose) polymerase. Nature 2005;434:913-7.
- Farmer H, McCabe N, Lord CJ, Tutt AN, Johnson DA, Richardson TB, et al. Targeting the DNA repair defect in BRCA mutant cells as a therapeutic strategy. Nature 2005;434:917–21.
- van den Berg J, G Manjón A, Kielbassa K, Feringa FM, Freire R, Medema RH. A limited number of double-strand DNA breaks is sufficient to delay cell cycle progression. Nucleic Acids Res 2018;46:10132–44.
- Jiang J, Chen Y, Zhang L, Jin Q, Wang L, Xu S, et al. i-CRISPR: a personalized cancer therapy strategy through cutting cancer-specific mutations. Mol Cancer 2022;21:164
- Kwon T, Ra JS, Lee S, Baek IJ, Khim KW, Lee EA, et al. Precision targeting tumor cells using cancer-specific InDel mutations with CRISPR-Cas9. Proc Natl Acad Sci U S A 2022;119:e2103532119.
- Tan IL, Perez AR, Lew RJ, Sun X, Baldwin A, Zhu YK, et al. Targeting the noncoding genome and temozolomide signature enables CRISPR-mediated glioma oncolysis. Cell Rep 2023;42:113339.
- Zou RS, Marin-Gonzalez A, Liu Y, Liu HB, Shen L, Dveirin RK, et al. Massively parallel genomic perturbations with multi-target CRISPR interrogates
 Cas9 activity and DNA repair at endogenous sites. Nat Cell Biol 2022;24:
 1433–44.
- Schindele A, Gehrke F, Schmidt C, Röhrig S, Dorn A, Puchta H. Using CRISPR-Kill for organ specific cell elimination by cleavage of tandem repeats. Nat Commun 2022;13:1502.
- Zhang L, Zuris JA, Viswanathan R, Edelstein JN, Turk R, Thommandru B, et al. AsCas12a ultra nuclease facilitates the rapid generation of therapeutic cell medicines. Nat Commun 2021;12:3908.

- Martino J, Siri SO, Calzetta NL, Paviolo NS, Garro C, Pansa MF, et al. Inhibitors of Rho kinases (ROCK) induce multiple mitotic defects and synthetic lethality in BRCA2-deficient cells. Elife 2023;12:e80254.
- Wie M, Khim KW, Groehler Iv AS, Heo S, Woo J, Son K, et al. Alkylation of nucleobases by 2-chloro-N,N-diethylethanamine hydrochloride (CDEAH) sensitizes PARP1-deficient tumors. NAR Cancer 2023;5:zcad042.
- Fujii M, Shimokawa M, Date S, Takano A, Matano M, Nanki K, et al. A
 colorectal tumor organoid library demonstrates progressive loss of niche factor
 requirements during tumorigenesis. Cell Stem Cell 2016;18:827–38.
- Konermann S, Brigham MD, Trevino AE, Joung J, Abudayyeh OO, Barcena C, et al. Genome-scale transcriptional activation by an engineered CRISPR-Cas9 complex. Nature 2015;517:583–8.
- Gasperini M, Hill AJ, McFaline-Figueroa JL, Martin B, Kim S, Zhang MD, et al. A genome-wide framework for mapping gene regulation via cellular genetic screens. Cell 2019;176:377–90.e19.
- Young CS, Hicks MR, Ermolova NV, Nakano H, Jan M, Younesi S, et al. A single CRISPR-Cas9 deletion strategy that targets the majority of DMD patients restores dystrophin function in hiPSC-derived muscle cells. Cell Stem Cell 2016;18:533–40.
- Kim HK, Kim Y, Lee S, Min S, Bae JY, Choi JW, et al. SpCas9 activity prediction by DeepSpCas9, a deep learning-based model with high generalization performance. Sci Adv 2019;5:eaax9249.
- Shen MW, Arbab M, Hsu JY, Worstell D, Culbertson SJ, Krabbe O, et al. Predictable and precise template-free CRISPR editing of pathogenic variants. Nature 2018;563:646–51.
- Fu Y, Foden JA, Khayter C, Maeder ML, Reyon D, Joung JK, et al. Highfrequency off-target mutagenesis induced by CRISPR-Cas nucleases in human cells. Nat Biotechnol 2013;31:822–6.
- Hsu PD, Scott DA, Weinstein JA, Ran FA, Konermann S, Agarwala V, et al. DNA targeting specificity of RNA-guided Cas9 nucleases. Nat Biotechnol 2013;31:827–32.
- Concordet JP, Haeussler M. CRISPOR: intuitive guide selection for CRISPR/ Cas9 genome editing experiments and screens. Nucleic Acids Res 2018;46:W242-5.
- Kim S, Kim D, Cho SW, Kim J, Kim JS. Highly efficient RNA-guided genome editing in human cells via delivery of purified Cas9 ribonucleoproteins. Genome Res 2014;24:1012–9.
- Akcakaya P, Bobbin ML, Guo JA, Malagon-Lopez J, Clement K, Garcia SP, et al. In vivo CRISPR editing with no detectable genome-wide off-target mutations. Nature 2018;561:416–9.
- Jang DE, Lee JY, Lee JH, Koo OJ, Bae HS, Jung MH, et al. Multiple sgRNAs with overlapping sequences enhance CRISPR/Cas9-mediated knock-in efficiency. Exp Mol Med 2018;50:1–9.
- Zuo E, Cai YJ, Li K, Wei Y, Wang BA, Sun Y, et al. One-step generation of complete gene knockout mice and monkeys by CRISPR/Cas9-mediated gene editing with multiple sgRNAs. Cell Res 2017;27:933–45.
- Wei T, Cheng Q, Min YL, Olson EN, Siegwart DJ. Systemic nanoparticle delivery of CRISPR-Cas9 ribonucleoproteins for effective tissue specific genome editing. Nat Commun 2020;11:3232.
- 35. Höijer I, Emmanouilidou A, Östlund R, van Schendel R, Bozorgpana S, Tijsterman M, et al. CRISPR-Cas9 induces large structural variants at on-target

- and off-target sites in vivo that segregate across generations. Nat Commun 2022:13:627.
- Tsai HH, Kao HJ, Kuo MW, Lin CH, Chang CM, Chen YY, et al. Whole genomic analysis reveals atypical non-homologous off-target large structural variants induced by CRISPR-Cas9-mediated genome editing. Nat Commun 2023;14:5183.
- Mao Z, Bozzella M, Seluanov A, Gorbunova V. DNA repair by nonhomologous end joining and homologous recombination during cell cycle in human cells. Cell Cycle 2008;7:2902–6.
- 38. Ray Chaudhuri A, Nussenzweig A. The multifaceted roles of PARP1 in DNA repair and chromatin remodelling. Nat Rev Mol Cell Biol 2017;18:610–21.
- Zheng F, Zhang Y, Chen S, Weng X, Rao Y, Fang H. Mechanism and current progress of Poly ADP-ribose polymerase (PARP) inhibitors in the treatment of ovarian cancer. Biomed Pharmacother 2020;123:109661.
- Kim D, Nam HJ. PARP inhibitors: clinical limitations and recent attempts to overcome them. Int J Mol Sci 2022;23:8412.
- Cho SW, Kim S, Kim Y, Kweon J, Kim HS, Bae S, et al. Analysis of off-target effects of CRISPR/Cas-derived RNA-guided endonucleases and nickases. Genome Res 2014;24:132–41.

- Shen B, Zhang W, Zhang J, Zhou J, Wang J, Chen L, et al. Efficient genome modification by CRISPR-Cas9 nickase with minimal off-target effects. Nat Methods 2014;11:399–402.
- Pavani R, Tripathi V, Vrtis KB, Zong DL, Chari R, Callen E, et al. Structure and repair of replication-coupled DNA breaks. Science 2024; 385:eado3867.
- Cheng Q, Wei T, Farbiak L, Johnson LT, Dilliard SA, Siegwart DJ. Selective organ targeting (SORT) nanoparticles for tissue-specific mRNA delivery and CRISPR-Cas gene editing. Nat Nanotechnol 2020;15:313–20.
- Banskota S, Raguram A, Suh S, Du SW, Davis JR, Choi EH, et al. Engineered virus-like particles for efficient in vivo delivery of therapeutic proteins. Cell 2022;185:250–65.e16.
- Segel M, Lash B, Song J, Ladha A, Liu CC, Jin X, et al. Mammalian retroviruslike protein PEG10 packages its own mRNA and can be pseudotyped for mRNA delivery. Science 2021;373:882–9.
- Hamilton JR, Chen E, Perez BS, Sandoval Espinoza CR, Kang MH, Trinidad M, et al. In vivo human T cell engineering with enveloped delivery vehicles. Nat Biotechnol 2024;42:1684–92.

2904 Cancer Res; 85(15) August 1, 2025 CANCER RESEARCH